Int. J. Electrochem. Sci., 2 (**2007**) 523 - 533

International Journal of ELECTROCHEMICAL SCIENCE
www.electrochemsci.org

Mechanically milled Ru_xFe_y Electrocatalyst for Oxygen Reduction in acid media

P. Sotelo-Mazón[1,2], R.G. González-Huerta[2], J. G. Cabañas-Moreno[2], O. Solorza-Feria[1,]*

[1]Depto. Química, Centro de Investigación y de Estudios Avanzados del IPN, A. Postal 14-740, 07360 México D.F., México
[2]Instituto Politécnico Nacional, ESFM, Unidad Prof. ALM, México, D. F., 07738, México
[*]E-mail: osolorza@cinvestav.mx

Received: 6 June 2007 / *Accepted:* 22 June 2007 / *Published:* 1 July 2007

Electrocatalytic oxygen reduction reaction (ORR) on Ru_xFe_y fine particles prepared by mechanical milling was investigated in a sulfuric acid electrolyte. The activity of the catalysts with Vulcan carbon powder dispersed into a Nafion film coated on a glassy carbon (ink-type electrode) was studied by using the rotating disk electrode technique, RDE. Polarization measurements showed that the ORR occurs through a first order reaction with respect to oxygen with a mechanism involving four electrons transfer to water formation. A Tafel slope of *ca.* 0.120 V dec^{-1}, and an exchange current density of 5.08 x 10^{-5} mA cm^{-2} was deduced from the mass transfer corrected polarization curves. The kinetic parameters were compared with commercial electrocatalysts and are in agreement with previous results for other types of Ru-based electrocatalysts, prepared in organic solvents.

Keywords: Oxygen reduction; Mechanical milling; Ru-Fe electrocatalyst; catalytic activity

1. INTRODUCTION

Interest in fuel cells technology has motivated research on the synthesis and characterization of inexpensive materials that can accomplish the direct four-electron molecular oxygen reduction to produce water. The oxygen reduction reaction (ORR) is the key electrochemical reaction in the fuel cell operating at low temperature such as polymer electrolyte fuel cells (PEFC) and in cathodic reactions in metal-air batteries [1]. Even with the widely used platinum-based catalysts, the ORR is kinetically slow and leads to a higher reduction overpotential, due to the fact that the oxygen-oxygen bond (O-O) in the dioxygen molecule requires a higher bond dissociation energy. Over the years, alternative electrocatalysts for ORR, such as platinum-free metal combinations [2], metal oxides [3], organometallic complexes [4], and nanostructured materials such as ruthenium-based compounds [5-8], have been investigated. The incorporation of a chalcogenide to the ruthenium catalyst provides superior performance and stability in acid environment compared to a ruthenium catalyst alone.

However, the nondissolved or nonincorporated chalcogenide represents a source of contamination which should be avoided in the PEFC. An alternative to pure nanometric Pt be using Fe-based catalysts [9,10], because they display convenient activity and stability and also an enhancement of the ORR in H_2SO_4 solution at 25°C as has been reported when using an Fe-Pt alloy [11]. The reported decreasing overpotential at the cathode electrode could be attributed to addition of the more electronegative metal such as Fe to the platinum. Bimetallic and alloy catalysts have been a particularly active area of research in relation to low-temperature fuel cells. In this connection a Ru_xFe_y electrocatalyst would be a suitable candidate as a cathode electrode material for the multi-electron charge transfer process for water formation if this electrocatalyst were to possess long term chemical and electrochemical stability as expected.

In this paper, the effect of finely mixing Ru with Fe on the ORR activity in 0.5 M H_2SO_4 solution is investigated. Unsupported Ru_xFe_y nanoparticles were prepared by mechanical milling (MM) and used in physical characterization and dispersed in Vulcan carbon for electrochemical analyses. The kinetic studies of the catalysts for the ORR were done using a rotating disk electrode (RDE) technique and the results compared with those from commercial Ru powder, Ru_xFe_y synthesized by chemical pyrolysis in an organic solvent and Pt 10wt%/C (E-TEK).

2. EXPERIMENTAL PART

2.1. Ru_xFe_y catalyst preparation

The initial materials were ruthenium sponge (Alpha Aesar, 99.5% nominal purity, 780 μm average particle size), and iron powders (Strem Chemicals, 99.9% nominal purity, 1-5 μm particle size). The initial powder mixture was introduced in a chromium-steel vial under inert atmosphere (argon or nitrogen) together with a small quantity of methanol (to prevent excessive powder agglomeration during milling). The mechanical alloying operation was performed by using a vibratory SPEX mill with a ball-to-powder weight ratio of 40:1. After numerous milling trials (for times of up to 10 h) it was found that Ru powders were highly abrasive and led to considerable contamination by debris from the mill vial (made of chromium tool steel). Therefore, although the initial powder mixture had a composition Ru-5 at% Fe, and a weight of 1 g, the final composition of the powders after milling was much richer in Fe, as reported below.

For the material used in the experiments here reported milling was performed for 1 h. After the predetermined milling time, the vial was opened under inert atmosphere and the as-milled powders were recovered by washing the vials and balls with methanol, decanting the resulting suspension and finally evaporating the remaining methanol at room temperature. The dried powders are referred hereafter as Ru_xFe_y MM, and were used for physical analysis and electrochemical studies.

2.2. Physical characterization

X-ray diffraction (XRD) was employed to determine the phases present in the powders before

and after milling. A D500 diffractometer (Siemens) with CoKα radiation (λ = 1.789007 nm) was used for this purpose. In addition, scanning electron microscopy (SEM) and energy dispersive X-ray spectrometry (EDXS) were used to characterize powder size and morphology, and average and local chemical compositions, respectively. This was done in a Sirion FEG-SEM (from FEI) equipped with a Genesis 4000 microanalysis system (from EDAX).

2.3. Electrode preparation for RDE study and electrochemical set-up

In all the electrochemical studies glassy carbon disks with a cross-sectional area of 0.38 cm^2 and thickness of 5 mm were used as a support of the thin films and as working electrodes. Each disk was placed in a cup of an electrode holder made of Nylamid with a stainless steel base. Ink-type electrodes were prepared as follows: 5 mg of catalyst was dispersed on a 5 mg of Vulcan carbon and added to an ethylic alcoholic solution (140 μL) containing 20 μL of 5 wt % Nafion® (Du Pont, 1100 EW). The resulting mixture was sonicated for 5 min and 10 μL of the resulting catalytic ink was deposited onto the glassy carbon surface of the working electrode.

The electrochemical measurements were performed by using the conventional single compartment of a three-electrode array. The cyclic voltammetry and the rotating disk electrode (RDE) studies were performed in a potenciostat/galvanostat (EG&G Mod. 273A) and a Pine MSRX rotation speed controller. A platinum mesh was used as the counter electrode and Hg/Hg_2SO_4/0.5 M H_2SO_4 (MSE = 0.680V/NHE) as the reference electrode, placed outside the cell, kept at room temperature and connected by a porcelain Lugging capillary. All potentials are referred to NHE. A 0.5 M H_2SO_4 electrolyte (pH= 0.3) was prepared from double-distilled water. Prior to electrochemical measurements the acid electrolyte was degassed with nitrogen for the activation of the working electrode. Thereafter, the acid electrolyte was saturated with pure oxygen and maintained on the electrolyte surface during the electrochemical experiments. Hydrodynamic experiments were recorded in the rotation rate range of 100-1600 rpm at 5 mV s^{-1}.

3. RESULTS AND DISCUSSION

3.1. Characterization of the prepared Ru_xFe_y MM catalysts

Figure 1 shows the X-ray diffraction patterns from the original powder mixture (before milling) and after the powders had been milled for 1 hour. The original powder mixture produces well defined diffraction peaks corresponding to the phases Ru and α-Fe (Fig. 1a), although the latter displays considerable lower intensity due to the small initial Fe content (and the large difference in diffracting power between Fe and Ru). On the other hand, the diffraction pattern from the as-milled powders (Fig. 1b) is formed by much broader peaks, which still can be clearly identified as belonging to the Ru phase. In this case, however, the diffraction peaks from the α-Fe phase are not clearly recognized because they have become overlapped with those from Ru due to peak broadening. Only the peak of maximum intensity from α-Fe (nominally centered at about 52.2°, Fig. 1a), seems to be detected from

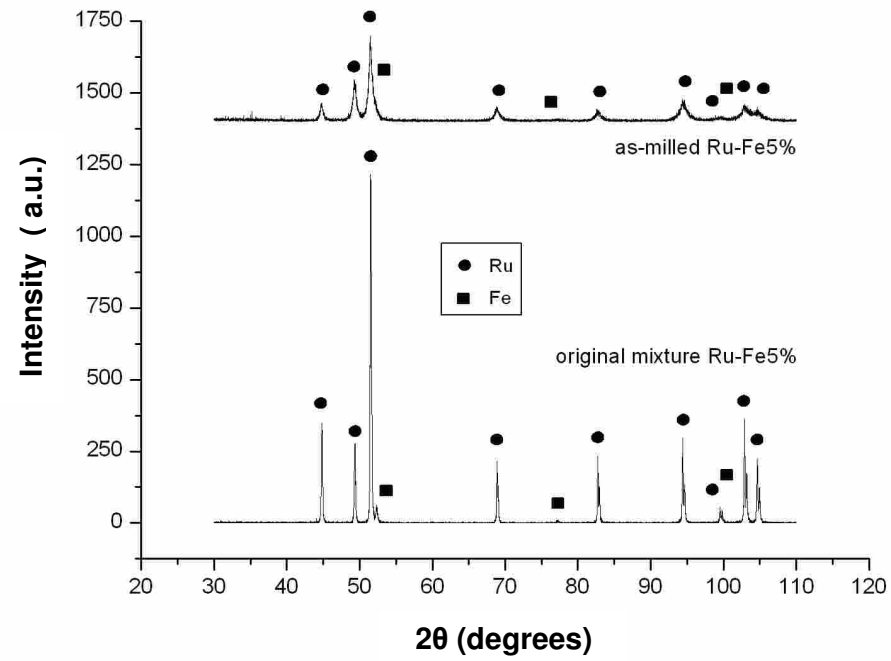

Figure 1. XRD patterns of the original Ru:Fe powder mixture (before milling) and after the powders had been milled for 1 hour.

its effect on the shape of the adjacent peak from the Ru phase, which becomes somewhat asymmetrical.

These results from XRD indicate that the short milling time used was only enough to produce a fine mixing of both metals, without the formation of significant quantities of a solid solution. Notice that no intermetallic phases are expected to be formed between Ru and Fe, according to the equilibrium phase diagram [12]. Milling apparently also led to a substantial reduction in the crystallite size of both phases, as suggested by the observed peak broadening. A rough estimate of the average crystallite size *d* in the Ru particles is 16 nm, as calculated by means of the Scherrer equation:

$$d = 0.9\lambda / B\cos\theta \qquad (1)$$

where λ is the X-ray wavelength, B the full width at half maximum of the diffraction peak (we used the 110 diffraction peak from Ru for the calculation, as this peak did not overlap with any possible α-Fe peaks in the diffraction pattern) and θ the Bragg diffraction angle. This value is most likely an underestimate of the true crystallite size (the Scherrer equation assumes negligible peak broadening from other sources), but it does indicate a rather fast reduction of crystallite size.

The morphology of the as-milled powders is observed on the SEM micrograph included in Figs. 2(a). At this low magnification the powders appear as irregular agglomerates of widely different sizes, the larger ones reaching 30 – 40 μm, while the smallest size observed is about 1 μm. Some surfaces on these agglomerates have a flat appearance, while the majority of surfaces are clearly irregular and rough. The difference is explained by the fact that during milling the powders can be

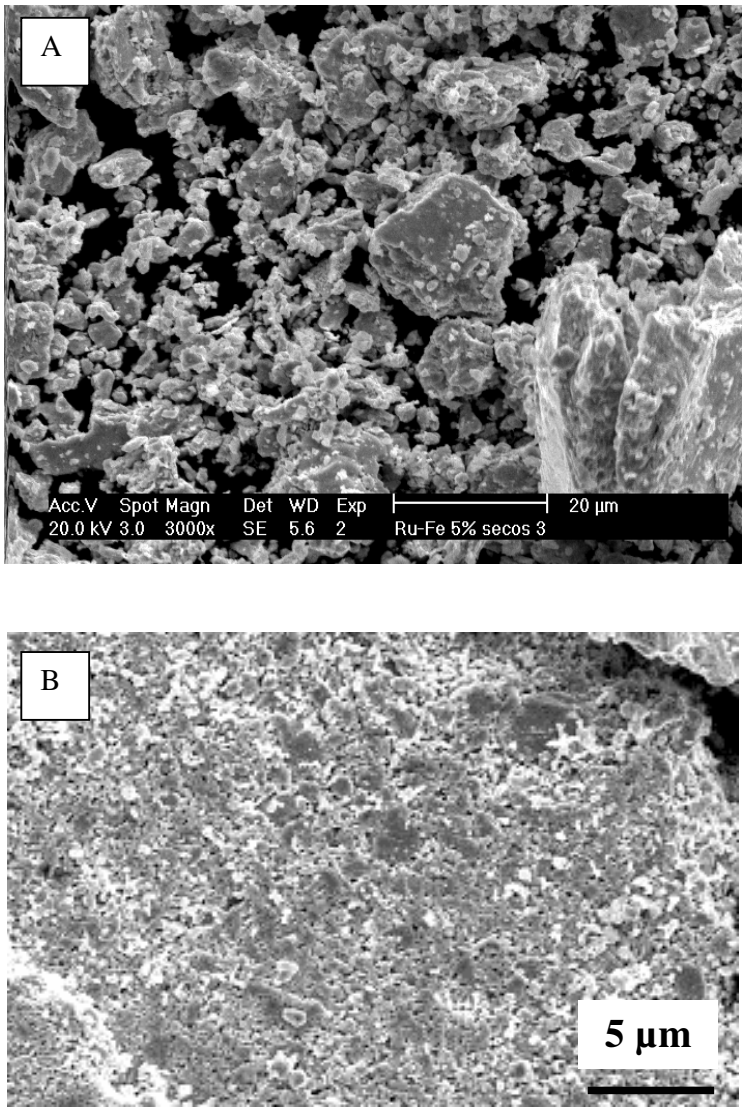

Figure 2. SEM micrographs of the as-milled powders.

compacted against the walls of the vial, thus producing the flat surfaces, but these compacted powders or agglomerates are also continuously broken down repeatedly due to the milling action, and the "fracture" surfaces of the agglomerates will have a highly irregular topography. The actual particle size in the powder agglomerates is revealed at higher magnification, as illustrated in Fig. 2b. This SEM micrograph clearly shows how one of the large powder agglomerates is composed of numerous powder particles having sizes of less than 0.5 microns. Notice that these particle sizes are still much larger than the calculated crystallite size (~ 16 nm), indicating that the particles are nanocrystalline, a common feature reported for metallic materials produced by the mechanical alloying process (12).

The average composition of the as-milled powders, as determined by EDXS, was approximately 67 at% Ru, 29 at% Fe and 4 at% Cr. As mentioned earlier, Ru powders proved to be highly abrasive during the milling operation, resulting in the contamination of the original powder mixture by the debris from balls and vials (made of chromium steel). In fact, the milling time chosen

represents a compromise between the compositional change of the powder mixture and the degree of mixing of the elemental powders.

These results of XRD and SEM-EDXS indicate that the as-milled powder mixtures consist mostly of powder agglomerates in which iron and ruthenium particles are intimately mixed, although some fraction of the iron content is present as dispersed Fe-rich particles.

3.2. RDE study of oxygen reduction

The oxygen reduction reaction is a complex combination of charge transfer and mass transport processes by which the low concentration of oxygen in acid environment is usually studied under hydrodynamic conditions. Figure 3 shows the hydrodynamic behavior of the Ru_xFe_y catalysts with Vulcan carbon powder dispersed into a Nafion film coated on a glassy carbon in oxygen saturated 0.5 M H_2SO_4 at 25 °C. The polarization curves were recorded from the open circuit potential to 0.2 V versus NHE. A charge-transfer kinetics control with rotation rate-independent current is observed in the range of 0.60-0.80 V/NHE; at more cathodic potentials, mixed control became significant without arriving to a well-defined mass transport-limited current as a function of the rotation rate. A similar behavior was

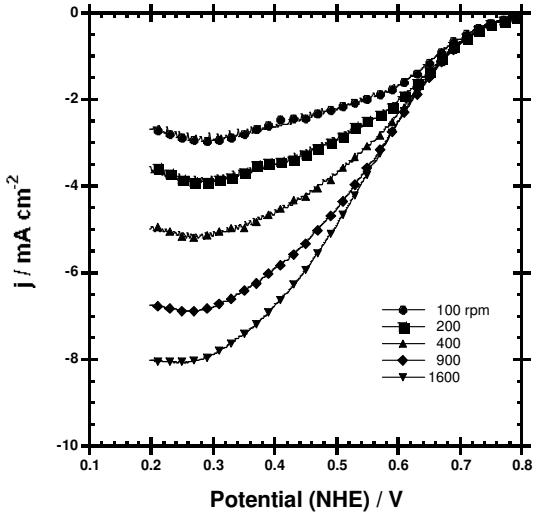

Figure 3. Hydrodynamic measurements for the ORR on a Ru_xFe_y catalyst in O_2-saturated 0.5M H_2SO_4 at 25°C, 5 mV s^{-1}. The current density was normalized to the geometric electrode area (0.38 cm^2).

observed for ruthenium nanoparticles [13] and a ruthenium chalcogenide cluster catalyst supported on carbon paste [14], that is, the potential regions under the mixed kinetic-diffusion control are clearly observed, regardless of the electrode rotation rates. It was considered that increases in the limiting current on high performance electrocatalysts are associated with the increase of molecular oxygen diffusion in the boundary layer thickness through the electrode surface. The reduction reaction is fast enough at high cathodic overpotentials, associated in almost all the cases to a flat limiting plateau as described for a Pt/C electrode [15]. An explanation for the well defined current plateau could be the

existence of a distribution of electrocatalytic sites on the electrode surface. When the distribution of active sites is less uniform and the electrocatalytic reaction is lower, the region of current plateau is limited, such as observed in Fig. 3.

Different electrode potentials were selected to determine the reaction order with respect to O_2, taking into account an estimated limiting current at each rotation rate [16,17]. The overall current, j , is related to the boundary-layer diffusion-limited current, j_d, and the reaction order, m, was calculated using equation (2):

$$\log\ j = m \log (1 - j / j_d) + \log j_k \qquad (2)$$

where m is deduced from the slope of the plot of $\log j$ vs. $\log(1 - j / j_d)$ at different rotation rates and different electrode potentials. j_k is the net kinetic current derived from the experimental current. Figure 4 presents this type of plot for the molecular oxygen reduction at a series of electrode potentials. As expected, the slopes of the straight lines in this plot are close to 1, which indicates that there is a single electron transfer to the electroreduced adsorbed oxygen on the electrode surface, this being the rate-determining step, i.e. $(O_2)_{ads} + H^+ + e^- \rightarrow (HO_2)_{ads}$ [18] The details of subsequent charge transfer reactions are unknown and may include several O_{ads} and OH_{ads} configurations.

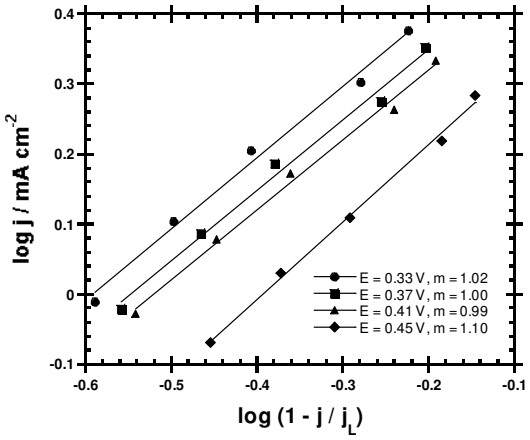

Figure 4. Reaction order plots for ORR on a Ru_xFe_y catalyst at various electrode potentials deduced from the data in Fig 3.

Also, the overall measured current, j , can be expressed as being dependent on the kinetic current , j_k , the boundary-layer diffusion-limited current, j_d, and film diffusion-limited current. However, as already described in our preceding publication (6) the resistance of the Nafion film which covers the dispersed catalyst is sufficiently small that can be neglected. Thus, the overall measured current density can generally be related by the Koutecky-Levich equation (relationship between j^{-1} versus $\omega^{-1/2}$) [19]:

$$\frac{1}{j} = \frac{1}{j_k} + \frac{1}{j_d} = \frac{1}{j_k} + \frac{1}{B\omega^{1/2}} \qquad (3)$$

j_d, can also be expressed in terms of the Levitch slope, B, by Eq. (4):

$$j_d = 0.2\, n\, F\, C_O\, D_O^{2/3}\, \nu^{-1/6}\, \omega^{1/2} = B\, \omega^{1/2} \qquad (4)$$

where 0.2 is a constant used when ω is expressed in revolutions per minute, n_e is the number of electrons transferred per molecule of O_2 in the overall reaction, F the Faraday constant, C_o the concentration of oxygen in the solution (1.1 x 10^{-6} mol cm^{-3}), D_o the diffusion coefficient of oxygen in the solution (1.4 x 10^{-5} cm^2 s^{-1}), and ν the kinematic viscosity of the sulfuric acid (1.0 x 10^{-2} cm^{-2} s^{-1}) [20]. At all the rotation speeds, as expected, a series of essentially parallel straight lines over a broad potential range is illustrated in Fig. 5. Parallelism of the straight lines in Fig. 5 indicates that the number of electrons transferred per O_2 molecule and the active surface area for the reaction do not change significantly within the potential range studied. For the Ru_xFe_y catalyst, the value of n_e was calculated to be ca. 4; similar multi-electron charge transfer processes were also obtained for other Ru-based compounds [13, 21-24]. From these results, we suggest that O_2 reduction may proceed via the overall four-electron transfer reaction for water formation, i.e., $O_2 + 4H^+ + 4e^- \rightarrow 2H_2O$, as has been reported under the same experimental conditions for transition-metal chalcogenides cluster compounds [22,25].

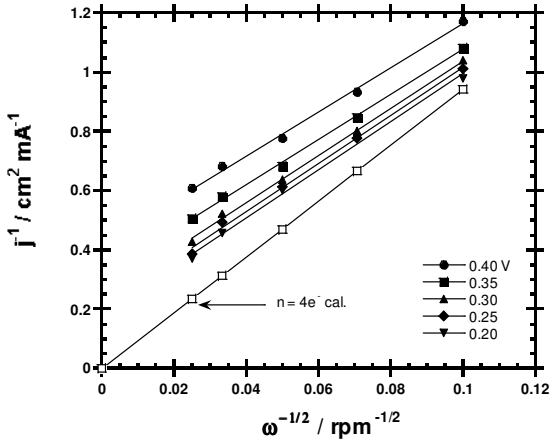

Figure 5. Koutecky-Levitch plots for the ORR on a Ru_xFe_y catalyst ink-type electrode at different electrode potentials obtained from the data in Fig 3.

Figure 6 shows the mass transport corrected Tafel plots obtained for the Ru_xFe_y catalyst ink-type electrode on which oxygen reduction kinetics studies were conducted in 0.5 M H_2SO_4 at 25 °C. The electrochemical activity found with the Ru_xFe_y catalyst prepared by mechanical milling (MM) is roughly similar to that encountered with a Ru_xFe_y catalyst synthesized by pyrolysis in 1,6 hexanediol [26], and different from the activity obtained with nanometric Ru and commercial Pt, which behavior is also depicted for comparison in Fig. 6. The Tafel plots were obtained after the measured currents were corrected for diffusion to give the kinetic currents in the mixed activation-diffusion region, calculated from equation 5:

$$j_k = j\ j_d\ /\ (j_d - j) \qquad (5)$$

Table 1. Kinetic parameters deduced from the Tafel slope for the ORR on Ru-based catalysts and Pt in a 0.5 H_2SO_4 electrolyte at 25 °C.

Electrocatalysts	E_{oc} V / NHE	-b V dec^{-1}	α	j_o mA cm^{-2}
Ru powder, Strem	0.85	0.119	0.49	8.31×10^{-7}
Ru_x hexanediol	0.80	0.110	0.53	4.29×10^{-6}
Ru_xFe_y hexanediol	0.81	0.120	0.49	1.77×10^{-5}
Ru_xFe_y MM	0.81	0.120	0.47	5.08×10^{-5}
Pt 10 wt%/C-ETEK	0.96	0.077	0.70	8.47×10^{-5}

where $j_d/(j_d - j)$ is the mass transfer correction term. In all cases the Tafel plots show a linear behavior in the mixed activation-diffusion region and a deviations of the kinetic current were observed with higher slope at high current density, corresponding to the limitations imposed by mass transfer. It is also observed from the Tafel plots that the overpotential decreases by the addition of Fe, a more electronegative metal than Ru. The kinetic parameters deduced for the oxygen reduction on Ru-based and Pt catalyst ink-type electrodes prepared by mechanical milling, pyrolysis in 1,6 hexanediol and commercial Ru are presented in Table 1. There are no significant differences among the Tafel slopes, b, and transfer coefficients, α, corresponding to the Ru_xFe_y catalysts prepared by the two different techniques. The value of the Tafel slope obtained in both cases is close to -2.3x $2RT/F$ (one-electron-discharge determining step mechanism).

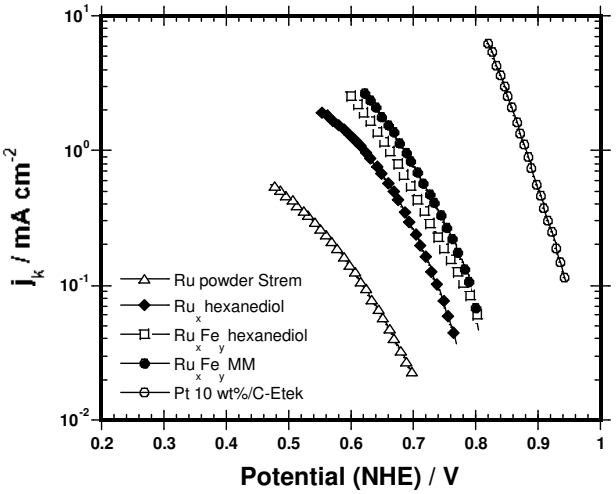

Figure 6. Tafel plots for the ORR on different Ru-based electrocatalysts in O_2-saturated 0.5 M H_2SO_4 at 25°C.

A difference in magnitude is observed in the exchange current density. This is probably due to the impurity content and powder morphology of the mechanically milled catalyst and also to the structure of the ink-type catalyst layer on the glassy carbon electrode. As shown in Fig. 2, it is seen that the catalyst particles adhered to each other to form larger particle agglomerates which lead to a reduction of active sites on the electrode surface. Consequently, a reduction on the exchange current density is obtained. However, the intrinsic electrochemical properties for the ORR of these bimetallic

surfaces have superior activity compared to pure ruthenium (13), which could be attributed to the bifunctional effect in which the unique catalytic properties of each of the elements in the binary compound combine in a synergetic fashion to yield a more active surface than each of the elements alone. However, Pt shows the better cathode performance in terms of catalytic activity toward four-electron reduction of oxygen to water in the acid environment.

4. CONCLUSIONS

The kinetic analysis revealed that the addition of Fe to Ru enhanced the catalytic activity of Ru for the ORR. The results deduced from the Tafel analysis suggest that the reduction of oxygen on the Ru_xFe_y electrocatalyst prepared by mechanical milling proceeds predominantly with the exchange of four electrons with a first order reaction with respect to the oxygen concentration. The performance achieved with the Ru_xFe_y (MM) cathode catalyst is related to the catalyst particle size and its distribution on the carbon surface.

ACKNOWLEDGEMENTS

This research project was financially supported by the National Science and Technology Council of Mexico, CONACYT, under grants No. 46094 and 48045 and by IPN (project 20060809). JGCM acknowledges a fellowship from COFAA-IPN.

References

1. L. Liu, H. Kim, J.-W. Lee and B. N. Popov, *J. Electrochem. Soc.*, 154 (2007) A123.
2. J.-H. Kim, A. Ishihara, S. Mitsushima, N. Kamiya and K.-I. Ota, *Electrochim. Acta*, 52 (2007) 2492.
3. L. Mao, D. Zhang, T. Sotomura, K. Nakatsu, N. Koshiba and T. Ohsaka, *Electrochim. Acta*, 48 (2003) 1015.
4. J. Pavez J, M. Paéz, A. Ringuedé, F. Bedioui and J.H. Zagal, *J. Sol. St. Electrochem*, 9 (2005) 21.
5. S. Durón S, R. Rivera-Noriega, P. Nkeng, G. Poillerat and O. Solorza-Feria, *J. Electroanal. Chem.*, 566 (2004) 281.
6. R.G. González-Huerta, J.A. Chávez-Carvayar and O. Solorza-Feria, *J. Power Sources*, 153 (2006) 11.
7. M. Bron, P. Bogdanoff, S. Fiechter, I. Dorbandt, M. Hilgendorhh, H. Schulenburg and H. Tributsch, *J. Electroanal. Chem.*, 500 (2001) 510.
8. V.I. Zaikovskii, K.S. Nagabhushana, V.V. Krivenskov, K.N. Loponov, S.V. Chereponova, R.I. Kvon, H. Boennemann, D.I. Kochuvey and E.R. Savinova, *J. Phys. Chem. B*, 110 (2006) 6881.
9. M. Lefèvre and J.-P. Dodelet, *Electrochim. Acta,* 48 (2003) 2749.
10. D. Villers, X. Jacques-Bédard and J.-P. Dodelet, *J. Electrochem. Soc.*, 151 (2004) A1507.
11. A.B. Anderson, J. Roques, S. Mukerjee, V.S. Murthi, N.M. Markovic and V. Stamenkovic, *J. Phys. Chem, B,* 109 (2005) 1198.
12. W.B. Pearson, Handbook of Lattice Spacing and Structures of Metals and Alloys. Vol. 2. National Research Council, Pergamon, Ottawa CA, 1992.

13. R.G. González-Huerta, R. Gonzalez-Cruz, S. Citalán-Cigarroa, C. Montero-Ocampo and O. Solorza-Feria, *J. New Mat. Electrochem. Systems*, 8 (2005) 15.
14. S. Durón, R. Rivera-Noriega, G. Poillerat and O. Solorza-Feria, *J. New Mat. Electrochem. Systems,* 4 (2001) 17.
15. U.A. Paulus, T.J. Schmidt, H.A. Gasteiger and R J. Behm, *J. Electroanal. Chem.*, 495 (2001) 134.
16. Yu V. Pleskov and Filinovskii, The Rotating Disc Electrode. New York, NY: Consultant Bureau, 1976.
17. S.K. Zecevic, J.S. Wainright, M.H. Litt, S. Lj. Gojkovic and R.F. Savinell, *J. Electrochem. Soc*., 144 (1997) 2973.
18. N.M. Markovic and P.N. Ross Jr, Interfacial Electrochemistry, Theory, Experiment and Applications, A. Wieckowsky ed., New York: Marcel Dekker, 1999.
19. A.J. Bard and L. Faulkner, Electrochemical Methods, Fundamentals and applications, New York, NY: Wiley & Sons; 2001.
20. C. Coutanceau, P. Crouigneau, J.-M Léger and C. Lamy, *J. Electroanal. Chem*., 379 (1994) 389.
21. R. González-Cruz and O. Solorza-Feria, *J. Sol. State Electrochem*., 7(2003) 289.
22. H. Tributsch, M. Bron, M. Hilgendorff, H. Schlenburg, I. Dorbandt, V. Eyert, P. Bogdanoff and S. Fiechter, *J. Appl. Electrochem.*, 31 (2001) 739.
23. T.J. Schmidt, U.A. Paulus, H. Gasteiger, N. Alonso-Vante, R. J.Behm, *J. Electrochem. Soc.*, 147 (2000) 2620.
24. J. Prakash and H. Joachin, *Electrochim. Acta,* 45 (2000) 2289.
25. S. Durón, R. Rivera-Noriega, M.A. Leyva, P. Nkeng, G. Poillerat and O. Solorza-Feria, *J. Sol. State Electrochem.*, 4 (2000) 70.
26. R. Rivera-Noriega, N. Castillo-Hernández, A.B. Soto-Guzmán and O. Solorza-Feria, *Int. J. Hydrogen Energy*, 27 (2002) 457.